Orientation of the Tetranuclear Manganese Cluster and Tyrosine Z in the O_2-Evolving Complex of Photosystem II: An EPR Study of the $S_2Y_Z^\bullet$ State in Oriented Acetate-Inhibited Photosystem II Membranes†

K. V. Lakshmi,‡ Sandra S. Eaton,§ Gareth R. Eaton,§ and Gary W. Brudvig*,‡

Department of Chemistry, Yale University, New Haven, Connecticut 06520-8107, and Department of Chemistry and Biochemistry, University of Denver, Denver, Colorado 80208

Received April 5, 1999; Revised Manuscript Received June 16, 1999

ABSTRACT: Inhibitory treatment by acetate, followed by illumination and rapid freezing, is known to trap the $S_2Y_Z^\bullet$ state of the O_2-evolving complex (OEC) in photosystem II (PS II). An EPR spectrum of this state exhibits broad split signals due to the interaction of the tyrosyl radical, $Y_Z^\bullet$, with the $S = 1/2$ S_2 state of the Mn_4 cluster. We present a novel approach to analyze $S_2Y_Z^\bullet$ spectra of one-dimensionally (1-D) oriented acetate-inhibited PS II membranes to determine the magnitude and relative orientation of the $S_2Y_Z^\bullet$ dipolar vector within the membrane. Although there exists a vast body of EPR data on isolated spins in oriented membrane sheets, the present study is the first of its kind on dipolar-coupled electron spin pairs in such systems. We demonstrate the feasibility of the technique and establish a rigorous treatment to account for the disorder present in partially oriented 1-D membrane preparations. We find that (i) the point-dipole distance between $Y_Z^\bullet$ and the Mn_4 cluster is 7.9 ± 0.2 Å, (ii) the angle between the interspin vector and the thylakoid membrane normal is 75°, (iii) the g_z-axis of the Mn_4 cluster is 70° away from the membrane normal and 35° away from the interspin vector, and (iv) the exchange interaction between the two spins is -275×10^{-4} cm^{-1}, which is antiferromagnetic. Due to the sensitivity of EPR line shapes of oriented spin-coupled pairs to the interspin distance, the present study imposes a tighter constraint on the Y_Z-Mn_4 point−dipole distance than obtained from randomly oriented samples. The geometric constraints obtained from the 1-D oriented sample are combined with published models of the structure of Mn-depleted PS II to propose a location of the Mn_4 cluster. A structure in which Y_Z is hydrogen bonded to a manganese-bound hydroxide ligand is consistent with available data and favors maximal orbital overlap between the two redox center that would facilitate direct electron- and proton-transfer steps.

Photosystem II (PS II) couples the oxidation of water to dioxygen with the reduction of plastoquinone in the photosynthetic electron-transfer chain in plants and cyanobacteria. The initial absorption of a photon produces a charge-separated P_{680}^+ $Pheo^-$ state. Stabilization of these species against charge recombination and maintenance of the quantum yield in PS II is efficiently achieved by the oxidation of $Pheo^-$ by Q_A and the reduction of P_{680}^+ by a tyrosine residue, Tyr_Z (Y_Z). Y_Z has been identified as Tyr-161 of the D1 polypeptide (cyanobacterial numbering) and is known to be the redox link between the Mn_4 cluster and P_{680}. The tetranuclear manganese cluster accumulates oxidizing equivalents by discrete electron-transfer steps to Y_Z. The Mn_4 oxidation states are described by the Kok S-state cycle (*1*) and a molecule of dioxygen is released during the fourth turnover via the S_4 state.

The active water-splitting site in PS II contains the Mn_4 cluster and Y_Z together with the required inorganic ions, Ca^{2+} and Cl^-. It is thought that, in addition to its role as a redox cofactor, Y_Z may be involved in proton-coupled electron transfer (*2*−*8*). Hoganson and Babcock (*3*) propose a metalloradical mechanism for O_2 evolution in PS II that is based on Tyr_Z acting as a hydrogen atom abstractor. The overall scheme involves the transfer of four electrons via the Y_Z tyrosyl radical and oxidation of two water molecules to produce dioxygen with the Mn_4 cluster acting as an electrically neutral catalytic site. In a related model, Britt and co-workers (*2*, *4*, *5*) propose that the close proximity of the Mn_4 cluster to Y_Z allows Y_Z to abstract protons from substrate water bound to the Mn_4 cluster. They suggest that rereduced $Y_Z^\bullet$ is a strong base and could extract a proton from a water molecule acidified by binding to a high-valence manganese ion in the cluster. On the basis of a consideration of the chemistry of Mn=O species, distributed dipole calculations, and model building, Brudvig and co-workers (*7*, *8*) propose that Y_Z is directly hydrogen bonded to a hydroxyl ligand on one of the di-μ-oxo Mn_2 dimers in the Mn_4 cluster, placing it close enough to a proximal manganese to participate in direct proton-coupled electron transfer, generating a catalytically active Mn^V=O species.

Determination of the distance and orientation between the Mn_4 cluster and Y_Z is crucial to unraveling the mechanism of proton- and electron-transfer events between the two

* To whom correspondence should be addressed: Phone: (203) 432-5202. Fax: (203) 432-6144. E-mail: Gary.Brudvig@Yale.Edu.

† This work was supported by Grants GM32715, GM36442 (Yale), and GM21156 (Denver) from the National Institutes of Health.

‡ Department of Chemistry, Yale University.

§ Department of Chemistry and Biochemistry, University of Denver.

10.1021/bi990780s CCC: $18.00
Published on Web 09/09/1999

cofactors. Inhibitory treatments on the donor side of PS II, followed by illumination and rapid freezing, are known to trap the protein in the $S_2Y_Z^\bullet$ state (*2*, *6*, *9*−*12*). The broad "split signal" EPR spectrum from the $S_2Y_Z^\bullet$ state, containing both the split $Y_Z^\bullet$ EPR signal as well as the S_2 multiline signal from the Mn_4 cluster, enables analysis of the exchange and dipolar interactions giving rise to this spectrum (*13*).

Structural information for PS II has been limited by the lack of well-ordered crystals. A recent 8 Å resolution electron crystallography structure of manganese-depleted plant photosystem II by Rhee et al. reveals the orientation of α-helices in the D1, D2, and CP47 polypeptides (*14*) but lacks critical data regarding the position and relative orientation of the Mn_4 cluster and Y_Z in the water-splitting active site. EPR spectroscopy is a powerful technique to characterize paramagnetic centers in bilayers and membranes. Analysis of cw EPR and electron spin−echo data for randomly oriented samples of $S_2Y_Z^\bullet$ have found a Mn_4-Y_Z interspin distance of 7.2−9.0 Å (*5*, *13*, *15*). In this system, the dominant contribution to the spin−spin interaction is the exchange coupling which makes evaluation of the dipolar coupling more difficult than if the dipolar interaction were dominant. However, exchange couplings are isotropic and thus examination of ordered samples provides a more accurate measure of the anisotropic dipolar interaction yielding better distance and orientation information than can be obtained from randomly oriented samples.

Previous EPR investigations of ordered membrane proteins (both single crystals and oriented membrane fragments) have targeted the arrangement of isolated EPR active redox cofactors in photosystems I and II (*16*−*35*). Dipolar spin−spin interaction in the EPR spectra of a PS I single crystal have been examined (*36*) and orientation selection in the tyrosyl radical EPR signal of PS II at high magnetic field permits analysis of dipolar interactions with other paramagnetic centers (*37*). Although EPR spectra of interacting paramagnetic centers in photosystem II samples oriented on Mylar films have been reported (*32*, *34*), the orientation-dependent spectra of dipolar coupled spin pairs have not been simulated previously. We present experimental and simulated $S_2Y_Z^\bullet$ spectra in oriented acetate-treated PS II membranes that determine the orientation of the $S_2Y_Z^\bullet$ dipolar vector with respect to the membrane normal. On the basis of the distance and orientation information derived in present study, we propose structural and functional models for the OEC in PS II.

MATERIALS AND METHODS

Preparation of Acetate-Treated Oriented PS II Membranes. PS II membrane fragments were isolated from spinach by previously published procedures (*38*), and O_2-evolution activities were found to be between 425 and 475 μmol of O_2/(mg of Chl h). Acetate-treated PS II membranes for the oriented $S_2Y_Z^\bullet$ experiments were resuspended in a buffer containing 10 mM 2-(*N*-morpholino)ethanesulfonic acid (Mes), 100 mM sodium acetate, and 10 mM calcium acetate at pH 5.5. *p*-Phenyl benzoquinone in dimethyl sulfoxide (DMSO) was added as an electron acceptor. Oriented samples were prepared by a single application of concentrated suspensions of PS II membranes ([Chl] > 12 mg/mL) on clean Mylar strips (25 × 2 × 0.03 mm, DuPont)

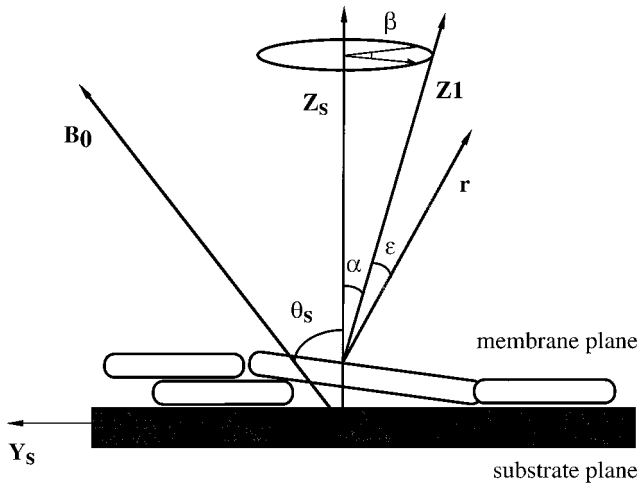

FIGURE 1: Schematic depicting the orientation of the axes. The angle θ_s describes the orientation of the substrate (mylar film) normal (Z_s) in the applied magnetic field (B_0). The Euler angles α and β define the orientation of z_1 (the Mn_4 *z*-axis) relative to the substrate normal, Z_s.

followed by equilibration for ∼10 h in a dark, 80% relative humidity chamber at 4 °C. Bundles of 3 or 4 Mylar strips were held together with Teflon holders, and the bundles were loaded into 4 mm quartz EPR tubes (Wilmad Glass). The total chlorophyll in an oriented sample is about 0.75 mg, which is only about 30% of the 2.5 mg present in typical frozen solution samples (*13*). The EPR tubes containing the Mylar bundles were sealed and frozen to 77 K. All manipulations were performed in the dark. Preillumination dark scans were obtained at 7.8 K. The sample was then illuminated at room temperature (500 W, white light) for 20 s, followed by rapid freezing at 77 K in the dark, to trap the $S_2Y_Z^\bullet$ state (*10*, *13*). After data acquisition as a function of orientation at 7.8 K, the samples were dark adapted for 45 min at 0 °C and refrozen at 77 K. Postillumination dark scans were then acquired and used in the subtractions to obtain light-minus-dark $S_2Y_Z^\bullet$ difference spectra.

EPR Spectroscopy. EPR measurements were performed on a Varian E-9 spectrometer, operating at 9.28 GHz, that is equipped with a TE_{102} cavity and an Oxford Instruments helium-flow cryostat. The long axis of the substrate (Y_S, Figure 1) is held vertically in the EPR sample tube. Rotation about the long axis of the EPR tube varies the orientation of the external magnetic field (B_0) within the Z_S-X_S plane of the substrate. The angle between B_0 and Z_S (the normal to the substrate plane) is defined as θ_S (Figure 1). The degree of orientation of the membrane fragments was assessed by monitoring the orientation dependence of the $Y_D^\bullet$ and cytochrome b_{559} (Cyt b_{559}) EPR signals (*17*) prior to room-temperature illumination. Spectra of $S_2Y_Z^\bullet$ shown in the figures are light-minus-dark difference spectra and the central (∼30 G) regions of the spectra are edited owing to interference from the dark-stable $Y_D^\bullet$ radical signal.

Spectral Simulations for Oriented EPR Signals. The electron−electron spin−spin interaction between the $S = 1/2$ Mn_4 cluster and $Y_Z^\bullet$ in the $S_2Y_Z^\bullet$ state of PS II gives rise to "AB" splitting patterns in the EPR spectrum (*13*, *39*). We previously simulated this "split" spectrum for randomly oriented samples using the program MnMeno (*13*). The equations in MnMeno were obtained by addition of manganese hyperfine coupling to Meno (*40*), which is based on

the work of Boas et al. (*41*). A modified version of MnMeno, OrMnMeno, was used to simulate the spectra of the 1-D ordered samples. This is the first example of simulations of dipolar-coupled electron spins in 1-D oriented membrane samples. The simulation includes Zeeman terms for the $S = 1/2$ Mn_4 cluster (H_{Z,Mn_4}) and the tyrosyl radical (H_{Z,Y_Z}), hyperfine coupling to the Mn_4 cluster (H_{A,Mn_4}), and dipolar (H_D) and isotropic exchange interactions (H_J) between the two paramagnetic centers:

$$H = H_{Z,Y_z} + H_{Z,Mn_4} + \sum_{i=1}^{4} H_{A,Mn_4} + H_D + H_J \quad (1)$$

where $H_Z \gg H_A \approx H_J \approx H_D$.

It is assumed that the **g**- and **A**-tensors for the Mn_4 cluster are coaxial. The nuclear hyperfine is treated as a perturbation: one ^{55}Mn nucleus is treated to second order and three ^{55}Mn nuclei are treated to first order. The exchange and dipolar interactions are treated as perturbations to second order. The exchange term is $-J\mathbf{S}_1\cdot\mathbf{S}_2$ and thus a negative value of J indicates antiferromagnetic interaction. The hyperfine couplings to the tyrosyl radical are smaller than the observed line widths of the signals for $S_2Y_Z^\bullet$ and so were not included in the calculations. The angles that define spatial relationships within the spin-coupled pair (see Figure 1 and ref *40*) are ϵ, angle between the interspin vector and the z_1 axis of the Mn_4 cluster; η, angle between the projection of the interspin vector on the x_1-y_1-plane of the Mn_4 cluster and the y_1 axis; $A1$, angle between the z_1 axis of the Mn cluster and the z_2 axis of the tyrosyl radical; and $A2$, angle between the projection of the z_2 axis on the x_1-y_1-plane and the x_1 axis. The approach to the 1-D ordering of the membranes that is used in OrMnMeno is analogous to that which was used by Schiller et al. to analyze EXAFS data for PS II samples on Mylar films (*42*). The orientation of the spin-coupled pair within the membrane is defined by α, the angle between the normal to the substrate, Z_S, and the z_1 axis of the Mn_4 cluster (Figure 1). It is assumed that the z_1 axis for the Mn_4 cluster has a well-defined orientation relative to the normal to the membrane. However, even in relatively well-oriented samples, there is variation (mosaic spread) in the orientation of the normal to the membrane relative to the normal to the substrate. The impact of the mosaic spread in orientations of the membrane normal on the effective orientation of z_1 is modeled as a Gaussian distribution in α. The width of the distribution, g_{wid}, is a variable in the simulation. The angle β defines the orientation of the projection of z_1 on the x_S-y_S plane of the substrate. This orientation is assumed to be random so simulations were performed by summing results for 95 values of β between 0 and 360°. The orientation of the external magnetic field relative to the normal to the substrate plane, θ_S, (Figure 1) is defined by the orientation of the sample in the cavity. The equations used in the simulations of the spin-coupled pair are written in terms of the orientation of the external magnetic field relative to the axes of the Mn_4 cluster, θ and φ. Axis transformation gives

$$\cos\theta = -\sin\theta_S \sin\alpha \cos\beta + \cos\theta_S \cos\alpha \quad (2)$$

$$\tan\varphi = (\sin\theta_S \sin\beta)/(\sin\theta_S \cos\alpha \cos\beta + \cos\theta_S \sin\alpha) \quad (3)$$

As noted by Schiller et al. (*42*), a distribution in α is not equivalent to a distribution in θ, because of the nonlinear relationship between α and θ shown in eq 2. The treatment of the mosaic as a distribution in the orientation of the membrane normal is a more rigorous way to analyze the EPR spectra than the previously used approach (*16*, *43*), in which the disorder was treated as a distribution in orientations of the magnetic field with respect to the axes of the paramagnetic center. A key factor in the simulations is the angle θ_D between the interspin vector and the normal to the substrate, which is given by

$$\cos\theta_D = -\sin\alpha \sin\epsilon \sin\eta + \cos\alpha \cos\epsilon \quad (4)$$

The **g** and **A** values for the Mn_4 cluster were based on the simulations of the spectra for the cluster in the absence of interaction ($g_x = g_y = 2.00$; $g_z = 1.91$; $A_x = A_y = 69.0 \times 10^{-4}$ cm^{-1}; $A_z = 87.0 \times 10^{-4}$ cm^{-1}; $A'_x = A'_y = 84.0 \times 10^{-4}$ cm^{-1}; $A'_z = 89.0 \times 10^{-4}$ cm^{-1}) (*13*) and the g values for $Y_Z^\bullet$ ($g_x = 2.007$; $g_y = 2.004$; $g_z = 2.002$) were taken from the high-field EPR study by Un et al. (*32*). Simulations were performed on Gateway 2000 P5-133 or Dell XPS R400 IBM-compatible computers.

RESULTS

X-band experimental EPR spectra of the $S_2Y_Z^\bullet$ signal in the 1-D oriented PS II membranes at 7.8 K are shown in Figure 2a (solid lines) for five orientations of the Mylar substrate relative to the external magnetic field. The dominant features in the spectra between 3000 and 3600 G are due to the "split" signal that arises from electron−electron spin−spin interaction between the $S = 1/2$ Mn_4 cluster and the tyrosyl radical. This interaction is dominated by the exchange contribution (*13*) and the resulting EPR signals can be understood by analogy with NMR AB splitting patterns (*39*, *44*). There is an AB splitting pattern due to interaction of the $Y_Z^\bullet$ signal with each hyperfine component of the spectrum of the Mn_4 cluster. Each line of the AB splitting pattern has contributions from both the Mn_4 cluster and $Y_Z^\bullet$; however, it is convenient to label the transitions based upon assignment in the limit as J goes to zero and r goes to infinity. For ^{55}Mn hyperfine components with resonance at a lower magnetic field than the $Y_Z^\bullet$ signal, the "inner" lines of the AB pattern for $Y_Z^\bullet$ (i_1, Figure 2a) are shifted to lower field than the noninteracting position and the less intense "outer" lines for $Y_Z^\bullet$ (o_1, Figure 2a) are shifted to higher field. Similarly, for ^{55}Mn hyperfine components with resonance at higher magnetic field, the $Y_Z^\bullet$ "inner" and "outer" lines (i_2 and o_2, Figure 2a) are shifted to higher and lower field, respectively, relative to the noninteracting signal. For each AB splitting pattern, the separations i_1-o_1 and i_2-o_2 are equal to the sum of the exchange and dipolar contributions to the electron−electron spin−spin interaction. The positions of all four lines depend both upon the spin−spin interaction and on the g values of the interacting spins. The ratios of signal intensities, i_1/o_1 and i_2/o_2, are determined by the ratio of the spin−spin splitting to the energy separation between the transitions for the Mn_4 cluster and $Y_Z^\bullet$ for a particular AB pattern. Thus, both the positions and relative intensities of the lines provide important constraints on simulations of the data (*13*).

The EPR spectra for randomly oriented samples are the superposition of AB patterns for all orientations of the spin-

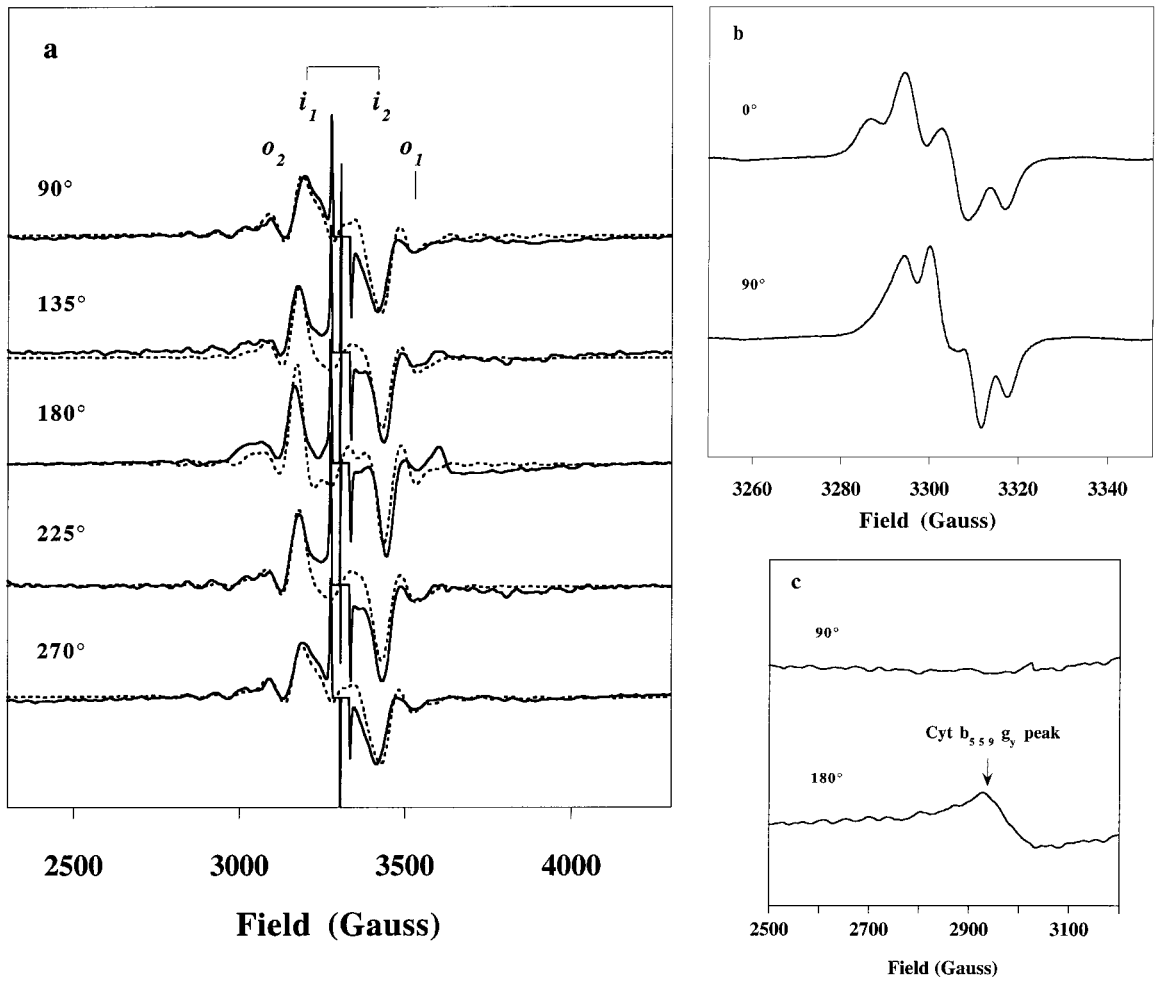

FIGURE 2: EPR signals from acetate-treated oriented PS II membranes. (a) Experimental $S_2Y_Z^\bullet$ spectra (solid lines) with θ_s, the angle between the substrate normal and the applied magnetic field, B_0, at 90, 135, 180, 225, and 270°, respectively. The central regions of ~30 G in these spectra have been deleted owing to the interference from the dark-stable tyrosyl radical, $Y_D^\bullet$, in PS II. Also shown are simulated $S_2Y_Z^\bullet$ spectra (dotted lines) at the same orientations as the experimental spectra. Simulations for oriented $S_2Y_Z^\bullet$ spectra with interacting $S = 1/2$ electron spins (Mn_4 and $Y_Z^\bullet$) were performed with the program OrMnMeno. (Experimental parameters) Microwave frequency = 9.28 GHz; magnetic field modulation frequency = 100 kHz; modulation amplitude = 20 G; microwave power = 20.0 mW; temperature = 7.8 K. (Simulation parameters) For Mn_4: $g_x = g_y = 2.00$; $g_z = 1.91$; $A_x = A_y = 69.0 \times 10^{-4}$ cm^{-1}; $A_z = 87.0 \times 10^{-4}$ cm^{-1}; $A'_x = A'_y = 84.0 \times 10^{-4}$ cm^{-1}; $A'_z = 89.0 \times 10^{-4}$ cm^{-1}; peak-to-peak line widths = 45 G. For $Y_Z^\bullet$: $g_x = 2.007$; $g_y = 2.004$; $g_z = 2.002$; peak-to-peak line widths = 35 G. For spin−spin interaction: $\alpha = 70°$; $\epsilon = 35°$; $r = 7.9$ Å; and $J = -275 \times 10^{-4}$ cm^{-1}. (b) EPR signals from the dark-stable tyrosyl radical, $Y_D^\bullet$, in acetate-treated oriented PS II membranes at $\theta_s = 0$ and 90°. At this microwave power there is some broadening of the signal due to power saturation. (Experimental parameters) Microwave frequency = 9.28 GHz; magnetic field modulation frequency = 100 kHz; modulation amplitude = 1.6 G; microwave power = 0.2 mW; temperature = 5.4 K. (c) The Cyt b_{559} g_y EPR signal in acetate-treated oriented PS II membranes at $\theta_s = 90$ and 180°. (Experimental parameters) Microwave frequency = 9.28 GHz; magnetic field modulation frequency = 100 kHz; modulation amplitude = 20 G; microwave power = 20.0 mW; temperature = 7.8 K.

coupled pair with respect to the external magnetic field. When the PS II membranes are oriented on the Mylar film, the orientation of the substrate in the external magnetic field restricts the range of orientations of the spin-coupled pairs relative to the external magnetic field. Thus, analysis of the orientation dependence of the spectra can be used to define the orientation of anisotropic tensors, including the dipolar tensor, relative to the normal to the substrate plane. To test the degree to which the PS II membrane samples were oriented, EPR spectra were recorded for the dark stable $Y_D^\bullet$ and the Cyt b_{559} g_y peak. These spectra were recorded prior to room-temperature illumination, for the samples that were used to study the $S_2Y_Z^\bullet$ signals. The spectra of $Y_D^\bullet$ obtained with the substrate normal parallel and perpendicular to the external field (Figure 2b) exhibit the orientation dependence of the hyperfine interaction that is characteristic of well-oriented membranes (*17*). The relative intensities of the Cyt b_{559} g_y peak when the substrate normal is perpendicular and parallel to the external field (Figure 2c) are comparable to those observed in previous EPR studies of oriented PS II membranes (*16*, *42*).

The positions of the i_1 and i_2 lines in the spectra of $S_2Y_Z^\bullet$ (Figure 2a) vary by 50 or 30 G, respectively, as a function of the orientation of the substrate in the external magnetic field (Figure 3). In addition, the observed line widths for both i_1 and i_2 are narrower when the external magnetic field is along the substrate normal ($\theta_S = 180°$) than at other orientations. These features of the spectra, in addition to the relative intensities of the inner and outer lines, were the characteristics that were monitored in seeking to match calculated spectra to the experimental data.

The parameters obtained previously by simulating X-band and Q-band spectra of randomly oriented samples of $S_2Y_Z^\bullet$ (*13*) were the starting points for the simulations of the

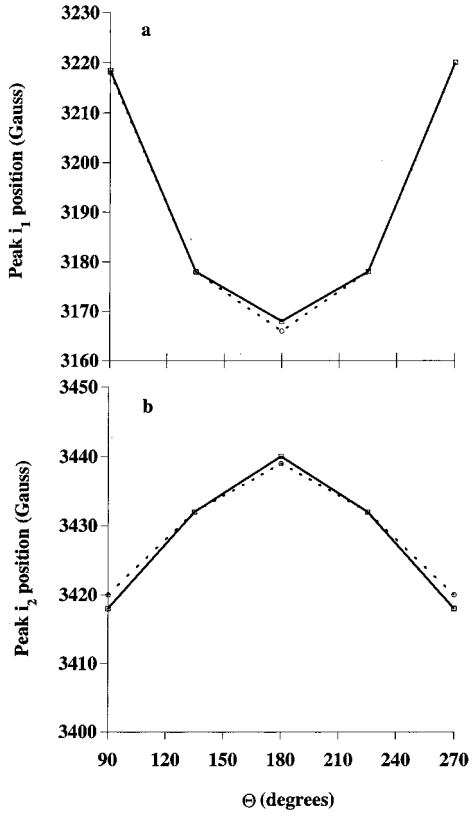

FIGURE 3: Rotation plots for the peak positions of (a) low-field inner line i_1 and (b) the high field inner line i_2 in experimental (solid lines) and simulated (dashed lines) oriented $S_2Y_Z^\bullet$ EPR signals.

oriented spectra: $r = 7.7$ Å, $J = -270 \times 10^{-4}$ cm^{-1}, $\epsilon < 35°$. A grid search was performed in which r, J, ϵ, η, and α were varied, and the simulations indicate that the spectra are quite sensitive to these parameters. The powder spectra do not depend on η (the angle between the projection of the interspin vector on the $x-y$ plane of the Mn cluster and the y axis of the cluster) because the **g**- and **A**-tensors are treated as axial (*13*). However, in the oriented samples, the orientation of the interspin vector relative to the normal to the substrate, θ_D, is defined in terms of η and therefore the simulated spectra depend on η. The best fit to the experimental data was obtained with $r = 7.9$ Å, $J = -275 \times 10^{-4}$ cm^{-1}, $\alpha = 70°$, $\epsilon = 35°$, and $\eta = 0°$; which corresponds to $\theta_D = 75°$. Spectra calculated with these parameters (dashed lines in Figure 2a) match the peak positions and the relative intensities of the inner and outer lines, as well as the variation of effective line widths with orientation. The orientation dependence of the positions of lines i_1 and i_2 calculated with these parameters is in good agreement with the experimental data (Figure 3). At $\theta_S = 180°$ (substrate normal aligned with the external magnetic field), there is greater discrepancy between the calculated and observed positions of i_1 and i_2. This discrepancy is attributed to interference from the signal from $Fe^{2+}Q_A^-$, which makes a maximal contribution at this orientation. Similar agreement was obtained between calculated and observed positions for the outer lines, o_1 and o_2 (data not shown). The estimated uncertainty in r based on the randomly oriented data was ± 0.5 Å, but the tighter constraints of the data for the oriented samples reduces the uncertainty to ± 0.2 Å. The uncertainties in α, ϵ, and J obtained from a similar grid search are ± 3°, ± 5°, and ± 10×10^{-4} cm^{-1}, respectively.

The width of the Gaussian distribution that was used in the simulations (Figure 2a) was 5°, although similar results are obtained with widths as high as 25°. A Gaussian width of 5−25° is consistent with the well-defined orientation dependence of the $Y_D^\bullet$ (Figure 2b) and Cyt b_{559} g_y (Figure 2c) signals observed in the dark-adapted oriented PS II membranes. The mosaic spread in the present study is comparable to the 23−35° spread estimated by Hasegawa et al. (*16*) and Schiller et al. (*42*) for PS II membranes oriented on Mylar films. The small **g** anisotropy for the tyrosyl radical ($g_x - g_z = 0.0054$) corresponds to a maximum variation of less than 9 G in resonance field as a function of orientation. This variation is too small to have a major impact on the simulated spectra so the data do not provide a definition of the orientation of the interspin vector relative to the axes of the tyrosyl radical.

The calculated dependence of the orientation-dependent spectra upon the value of θ_D is demonstrated in Figure 4. Figure 4a shows the orientation dependence of the EPR signal calculated for the same values of r and J as were used to simulate the experimental data, but with the values of α, ϵ, and η selected to give $\theta_D = 5°$. In this case when $\theta_S = 180°$, the direction of the external magnetic field is close to parallel to the interspin vector, and the maximum magnitude of dipolar coupling ($-2D$) is observed for all of the pairs in the sample. Because the Hamiltonian is expressed in terms of $-J$ and J is negative, the dipolar coupling at this orientation largely cancels the exchange interaction, the net spin−spin splitting is at a minimum, and the calculated positions of i_1 and i_2 are relatively close to that for noninteracting tyrosyl radical. When θ_D is small and the magnetic field is in the plane of the substrate ($\theta_S = 90$ and 270°), the minimum magnitude of dipolar coupling ($+D$) is observed for all of the pairs and the combined dipolar and exchange coupling reinforce, the spin−spin splitting is a maximum, and the calculated positions of i_1 and i_2 are shifted farthest from that for noninteracting tyrosyl radical. Figure 4b was calculated with the same values of r and J, but with α, ϵ, and η selected to give $\theta_D = 90°$. The spectra in Figure 4b exhibit substantially smaller orientation dependence than in Figure 4a because no value of θ_S aligns the external magnetic field with the interspin vector for all of the spins in the sample. The observed orientation dependence of the experimental data (Figure 2a) is closer to that shown in Figure 4b than in Figure 4a, which indicates that θ_D is closer to 90° than to 0°, in agreement with the assignment of $\theta_D = 75°$.

The best-fit simulation of the $S_2Y_Z^\bullet$ signal in a randomly oriented sample is obtained with ϵ (the angle between the interspin vector and the z axis of the Mn_4 cluster) values between 0 and 20° (*13*), but the best fit to the spectra of the 1-D oriented sample is obtained with ϵ equal to 35°. For the randomly oriented sample, the feature of the spectra that is most sensitive to ϵ is the manganese hyperfine splitting of the multiline signal (*13*). In the 1-D oriented sample, the value of ϵ is optimized based on the positions and orientation dependence of the split signal. In both simulations, it is assumed that the effective g axis for the Mn_4 cluster and the effective hyperfine axes for all four manganese nuclei are collinear and that the hyperfine splittings for three of the manganese nuclei are equivalent. The actual parameters are

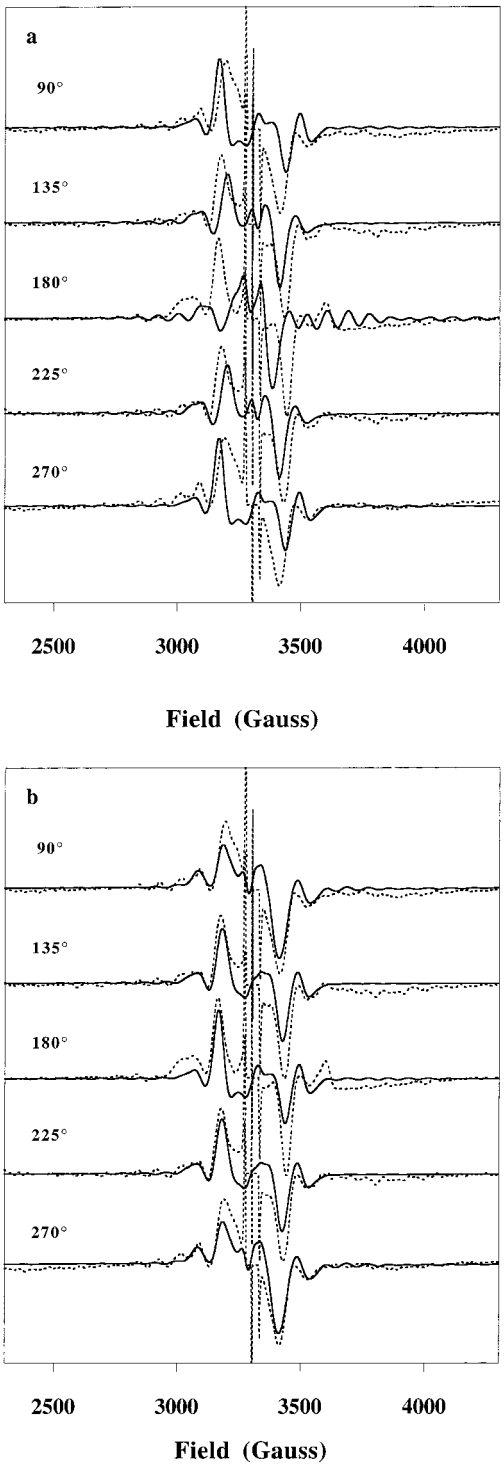

FIGURE 4: Simulated oriented $S_2Y_Z^{\bullet}$ spectra demonstrating the effect of θ_D on the peak positions and relative intensities of the split peaks (solid lines): (a) $\theta_D = 5°$ and (b) $\theta_D = 90°$. Also shown are the corresponding experimental spectra (dotted lines). (Experimental parameters) Same as Figure 2. (Simulation parameters) For Mn_4: $g_x = g_y = 2.00$; $g_z = 1.91$; $A_x = A_y = 69.0 \times 10^{-4}$ cm^{-1}; $A_z = 87.0 \times 10^{-4}$ cm^{-1}; $A'_x = A'_y = 84.0 \times 10^{-4}$ cm^{-1}; $A'_z = 89.0 \times 10^{-4}$ cm^{-1}; peak-to-peak line widths = 45 G. For $Y_Z^{\bullet}$: $g_x = 2.007$; $g_y = 2.004$; $g_z = 2.002$; peak-to-peak line widths = 35 G. For spin−spin interaction: (a) $\alpha = 5°$; $\epsilon = 0°$; $\eta = 0°$; $r = 7.9$ Å; and $J = -275 \times 10^{-4}$ cm^{-1}. (b) $\alpha = 90°$; $\epsilon = 0°$; $\eta = 90°$; $r = 7.9$ Å; and $J = -275 \times 10^{-4}$ cm^{-1}.

likely to be more complicated than assumed here and the uncertainties that arise due to the approximations may result in different optimized parameters depending on which features of the spin-coupled system are examined. As pointed out by Zheng and Dismukes (*45*), an analysis of the EPR spectra of the multiline signal that does not include any assumptions or approximations has too many adjustable parameters compared with the relatively small number of resolved features in the spectra. More extensive and resolved data for the multiline signal are required to refine the interpretation of the Mn_4 EPR spectrum. Because of the way the axis systems for the simulations were set up, the angle between the interspin vector and the normal to the membrane plane is defined in terms of ϵ. However, the best-fit value of η is 0°, so the angle ϵ is in a plane perpendicular to the plane that contains the normal to the membrane and the z_1 axis of the Mn_4 cluster. For this combination of angles, the value of θ_D is quite insensitive to the value of ϵ between 0 and 35°. Thus, the uncertainties concerning ϵ do not have a significant impact on θ_D.

The value of α, the orientation of the *z*-axis for the Mn_4 cluster relative to the normal to the membrane, that gives the best fit to the experimental data is 70°. The *z*-axis is assigned to the axis with the smallest *g* value. In a study of the S_2 multiline signal for 1-D oriented PS II membranes, Hasegawa et al. reported that the axis with the smallest *g* value is tilted at an angle of 51° relative to the membrane normal (*16*). Earlier, Kim et al. (*23*) reported that the axis with the smallest *g* value is at an intermediate angle relative to the membrane normal. The analysis of the multiline signal in each of these cases was based on different assumptions concerning the parameters for the Mn_4 cluster. These differences in assumptions, combined with the lack of a unique fit to the EPR spectrum, make it difficult to compare the results. However, it appears that the effective g_z axis for the cluster is neither collinear with nor perpendicular to the membrane normal. To relate the effective magnetic axes for the Mn_4 cluster to a physical dimension of the cluster requires a model of the magnetic coupling within the cluster, which remains the subject of considerable debate (*16*, *45*).

DISCUSSION

Previous EPR investigations of one-dimensionally ordered PS II membranes on Mylar films have focused mainly on the orientation of the **g**- and hyperfine tensors of isolated spins within the membranes (*16*, *17*, *19*−*21*, *23*, *34*). In the present study, we extend the repertoire of this technique to include a detailed investigation of dipolar-coupled electron spin pairs in PS II membranes. The analysis of the EPR spectra from the 1-D ordered samples as a function of the orientation of the sample in the external magnetic field permits determination of the angle θ_D between the interspin vector and the membrane normal, which cannot be obtained from spectra of randomly oriented samples. Simulations of the oriented samples also define the interspin distance, *r*, more precisely than can be obtained from randomly oriented samples (*13*). The values of θ_D and *r* provide key clues to the spatial orientation of Y_Z and the Mn_4 cluster which, when combined with other information in the literature, provides a clearer picture of the active water-splitting site in PS II.

The structure of PS II has been calculated based on the primary sequence of the protein, homology with the photosynthetic reaction center of Rps. *viridis*, and molecular mechanics calculations (*46*). The overall topology and

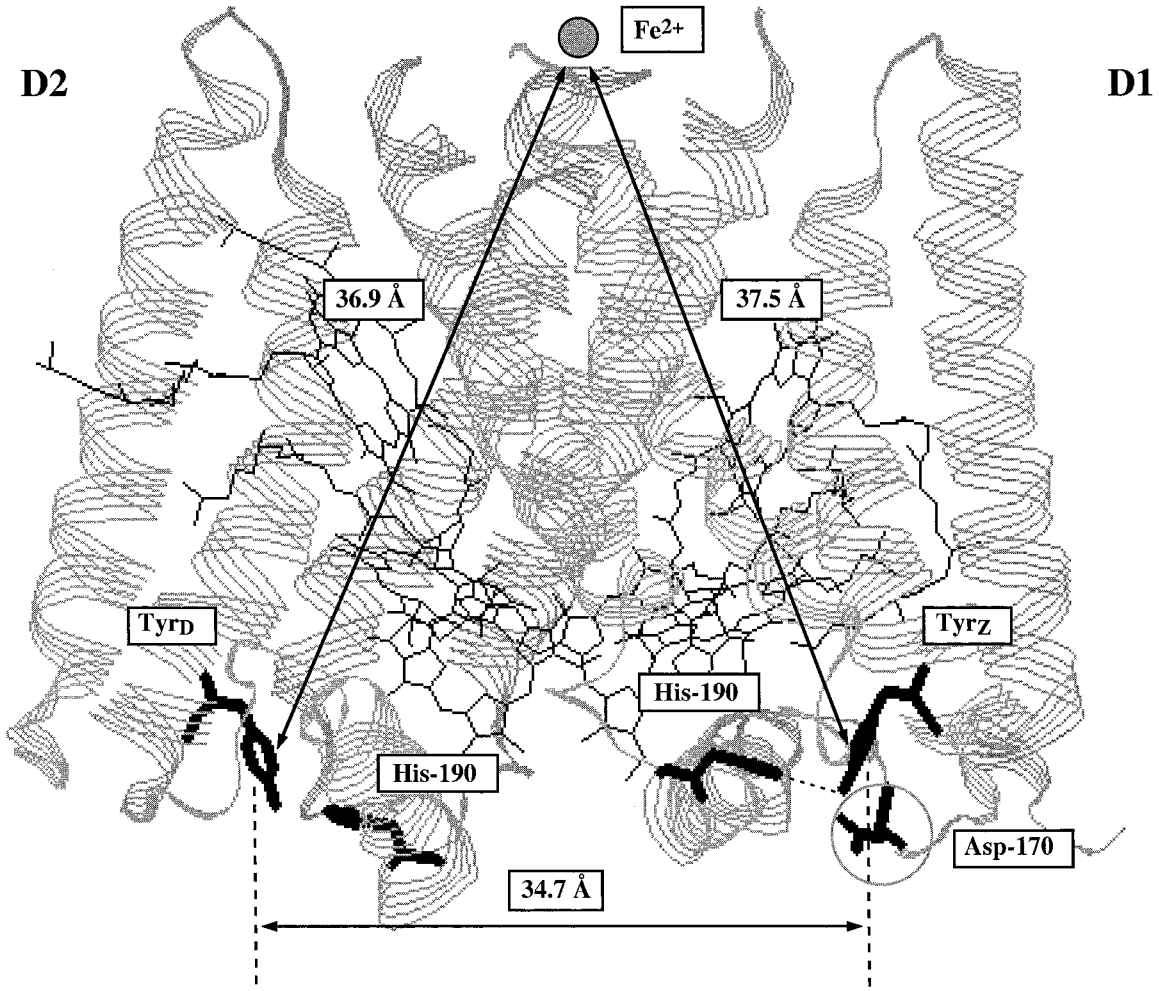

FIGURE 5: A model for the photosystem II reaction center core complex based on theoretical modeling by Styring and co-workers (46) highlighting the locations of the redox active tyrosine residues, Y_D and Y_Z; D2-His-190, a hydrogen-bonding partner to Tyr_D (74); as well as other key participants in water-oxidation, namely, D1-Asp-170 and D1-His-190.

organization of transmembrane helices in the calculated model is similar to that obtained by electron crystallography at 8 Å resolution for the photosystem II subcomplex containing proteins D1, D2, CP47, and Cyt b_{559} (*14*). The predicted model defines the location of key components of the photosynthetic system, including the redox-active tyrosyl residues Y_D and Y_Z (Figure 5). As discussed by Svensson et al. (*46*), the calculated distances between the non-heme iron, that lies near the top of helices from subunits D1 and D2, and the centers of the Y_Z and Y_D are 37.5 and 36.9 Å, respectively, which are in good agreement with the value of 37 ± 5 Å observed by EPR spin−lattice relaxation measurements (*47*, *48*). The calculated orientations of the C1−C4−O axis of the phenyl rings for both of the tyrosyl radicals (*46*) are consistent with EPR experiments that found orientations of about 70−90° from the membrane plane (*37*, *49*, *50*).

Also shown in Figure 5 are the locations of key amino acid residues in the D1 subunit [from the Svensson et al. model (*46*)] that are thought to be directly involved in water oxidation, namely, Tyr_Z, a redox active tyrosyl residue involved in proton-coupled electron-transfer; D1-His-190, a hydrogen-bonding partner to Tyr_Z; and D1-Asp-170, a proposed ligand to the Mn_4 cluster (*51*−*61*). Although Svensson et al. (*46*) note that the D1-Asp-170 side chain might provide a binding site to the Mn_4 cluster, the exact location of the cluster is not included in their model. On the basis of the protein coordinates of their model, the center of the tyrosyl ring of Y_Z is at a distance of 6.9 Å from the peptide backbone nitrogen atom on D1-Asp-170. However, there is considerable uncertainty in the side-chain orientation for D1-Asp-170, as this residue is protonated in the theoretical modeling to compensate for the absence of potential counterions. The possible positions of the carboxylate group allowed by rotation of the D1-Asp-170 side chain are within the circle shown in Figure 5. Taking this uncertainty into account, the Mn_4 cluster can be positioned at any location that allows D1-Asp-170 to be a ligand to one of the manganese ions in the cluster. Application of additional geometric constraints on the relative orientation of the Mn_4 cluster within the PS II membrane would enable a proposed representation of the complete water-splitting active site in PS II.

The present study addresses the spatial relationship between the Mn_4 cluster and Y_Z in the active site of PS II. The information obtained from analysis of the $S_2Y_Z^{\bullet}$ state of oriented acetate-treated PS II membranes concerning the orientation of the interspin vector and the distance between Y_Z and the Mn_4 cluster can be combined with data on the orientation of Y_Z (*37*, *49*, *50*) and the theoretical model of Svensson et al. (*46*) to define better the possible locations for the Mn_4 cluster. Figure 6 depicts the distance and angular constraints determined from the present study and the

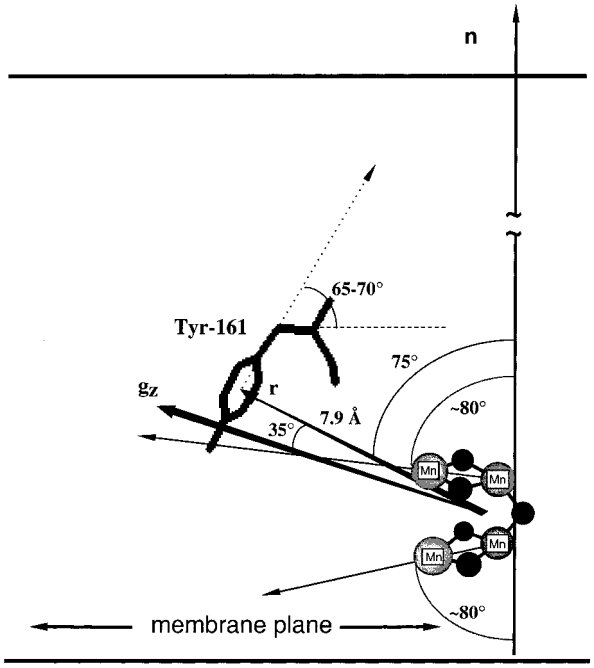

FIGURE 6: A model combining the location of Y_Z based on the predicted protein structure for PS II reaction centers (46) and the distance and relative orientation of the Mn_4 cluster and Y_Z within the membrane obtained from the EPR spectra of one-dimensionally ordered $S_2Y_Z^\bullet$ signals in acetate-treated PS II membranes. Also shown is a summary of related EXAFS and EPR structural data available to date on the Mn_4 cluster and $Y_Z^\bullet$ in the O_2-evolving center of PS II.

geometric constraints of the Mn_4 cluster and Y_Z within the membrane as determined by EXAFS and EPR experiments. In this model, the normal to the membrane is assumed parallel to the C_2 axis that relates the D1 and D2 subunits. On the basis of EXAFS data, the Mn_4 cluster is modeled as two di-μ-oxo bridged manganese binuclear structures with Mn−Mn separations of 2.7 Å, where the 2.7 Å vectors are approximately parallel to the membrane plane (*42*, *62*). As determined by a recent X-ray absorption linear-dichroism spectroscopy study of partially oriented PS II membranes, the orientation of the two 2.7 Å vectors with respect to the membrane normal is $\sim$ 80° with the individual angles different maximally by 14° (*42*). Although the representation in Figure 6 assumes that the Mn_4 cluster consists of two di-μ-oxo bridged dimers, we predict that the overall topography of the active site would be valid for other geometries of the Mn_4 cluster as well, with small uncertainties in the inter-residue distances.

A fit is then sought between the geometry of the Mn_4 unit and the protein coordinates of Svensson et al. (*46*), using the distance and orientation constraints provided by the 1-D oriented EPR spectra.[1] The 7.9 Å distance obtained from the EPR spectra is a point−dipole distance between the effective centers of the unpaired electron density on $Y_Z^\bullet$ and the Mn_4 cluster. For the tyrosyl radical, the electron density distribution has been found to be delocalized over the phenyl ring (*63*), and it is reasonable to use the center of the ring as the effective center for the delocalized spin. For the Mn_4 cluster, the interpretation of the spin delocalization depends on the assignment of the oxidation states and exchange couplings of the manganese in the cluster (*5*, *8*, *45*, *64*). As a first approximation for the purpose of this model, we assume a center-to-center $Mn_4-Y_Z^\bullet$ point−dipole distance where the centers of the manganese cluster and the tyrosyl ring are the effective centers for the delocalized spins on Mn_4 and $Y_Z^\bullet$, respectively. A detailed analysis of the distributed-dipole interaction between Mn_4 and $Y_Z^\bullet$ is in progress. The proposed structure with the $Mn_4-Y_Z^\bullet$ dipole vector fixed at an angle of 75° relative to the membrane normal (Figure 6), together with the $Y_Z - Y_D$ distance of 34.7 Å, gives a distance between Y_D and the center of the Mn_4 cluster of 39.5 Å, which is in reasonable agreement with the estimate of 25−35 Å obtained by Un et al. (*37*) and 22−40 Å by Brudvig and co-workers (*65*). Furthermore, placing the Mn_4 cluster within the geometric constraints determined in the present study of oriented PS II membranes places D1-Asp-170 in close enough proximity to the cluster to be a ligand to one of the manganese ions. This is in agreement with previous mutagenesis studies that suggest that Asp-170 in the D1 polypeptide is a putative ligand to the Mn_4 cluster (*52*, *66*, *67*) and manganese coordination chemistry and inorganic studies that indicate that the ligands to the Mn_4 cluster are primarily carboxylate residues in combination with μ-oxo or μ_2-hydroxo bridges (*68*−*70*). The 75° orientation of the $Mn_4-Y_Z^\bullet$ interspin vector relative to the membrane normal determined in this model is consistent with the spatial orientation and positioning of the Y_Z-containing helix in the D1 subunit of the PS II complex (*14*).

The structural model presented here is in agreement with the mechanistic proposals by Brudvig, Britt, and Babcock (*2*−*8*). The Babcock proposal (*3*) involves H-atom abstraction by $Y_Z^\bullet$ resulting in the oxidation of two water molecules with the Mn_4 cluster acting as an electrically neutral catalytic site. An independent model by Britt and co-workers (*2*, *4*, *5*) suggests that Y_Z^- is a strong base that could extract a proton from an acidic manganese-bound water/hydroxide ligand. The model of Brudvig and co-workers (*7*, *8*) proposes formation of a $Mn^V{=}O$ species in the Mn_4 cluster via two proton-coupled electron-transfer steps between $Y_Z^\bullet$ and a water molecule bound to the Mn_4 cluster. Although these proposals differ in detail, they have similar requirements; (i) that Y_Z be in close enough proximity to the Mn_4 cluster to be directly involved in an H bond with a bound water or hydroxide ligand on one of the manganese atoms, and (ii) that Y_Z also be involved in an H bond to a counterpartner (D1-His-190) that will accept the proton released during the oxidation of Y_Z. The combined model proposed in Figure 6 satisfies both of the above requirements in that the distance and relative orientation of the Mn_4 cluster and Y_Z favor H bonding between Y_Z and bound ligands on the cluster and the presence of D1-His-190 in close proximity to Tyr_Z would allow for Y_Z to release a proton upon oxidation that will subsequently be transferred to the bulk aqueous phase. Additional studies involving the oxidation states of the Mn_4

[1] Coordinates for the theoretical model of the photosynthetic reaction center from Spinach Photosystem II (core) were taken from the from the protein data bank (*72*, *73*) [entry 1DOP; Svensson, B., Etchebest, C., Tuffery, P., Van Kan, P., Smith, J., and S. Styring (1997)] (*53*) and were visualized using the software programs "Swiss-PDB viewer" (Glaxo Wellcome Experimental Research, Geneva, Switzerland) and RasMac 2.6-UCB1.0 (Roger Sayle, Glaxo Wellcome Research & Development, Hertfordshire, U.K.). The protein coordinates were used without further energy minimization. The Mn_4 cluster was constructed in "Chem 3D" (CambridgeSoft Corporation) and combined with the protein data file.

cluster in the S-state intermediates of the water-oxidation reaction in the OEC as well as characterization of oxygen-evolving manganese model systems (*71*) are necessary to resolve finer mechanistic aspects of the process.

The distance and relative orientation between the Mn_4 cluster and Y_Z supporting the presence of a hydrogen bond from a hydroxide/water ligand on the Mn_4 cluster to the tyrosyl (Y_Z) oxygen would, however, result in a much larger value of the exchange coupling (*J*) than is observed for the $S_2Y_Z^\bullet$ state in acetate-inhibited PS II samples (present study and ref *13*). The decreased magnitude of *J* observed in the acetate-treated samples (-275×10^{-4} cm^{-1}) indicates that acetate disrupts the hydrogen bonding between a ligand on the Mn_4 cluster and Y_Z and, in doing so, inhibits the donor side and traps the $S_2Y_Z^\bullet$ state. This would also account for the ENDOR finding that the distance between $Y_Z^\bullet$ and the methyl protons of a bound acetate ligand to the Mn_4 cluster is ~ 3 Å (*4*).

REFERENCES

1. Kok, B., Forbush, B., and McGloin, M. (1970) *Photochem. Photobiol. 11*, 457−475.
2. Gilchrist, M. L., Ball, J. A., Randall, D. W., and Britt, R. D. (1995) *Proc. Natl. Acad. Sci. U.S.A. 92*, 9545−9549.
3. Hoganson, C. W., and Babcock, G. T. (1997) *Science 277*, 1953−1956.
4. Force, D. A., Randall, D. W., and Britt, R. D. (1997) *Biochemistry 36*, 12062−12070.
5. Peloquin, J. M., Campbell, K. A., and Britt, R. D. (1998) *J. Am. Chem. Soc. 120*, 6840−6841.
6. Szalai, V. A., Kühne, H., Lakshmi, K. V., and Brudvig, G. W. (1998) *Biochemistry 37*, 13594−13603.
7. Limburg, J., Szalai, V. A., and Brudvig, G. W. (1999) *J. Chem. Soc., Dalton Trans.* 1353−1361.
8. Szalai, V. A., Stone, D. A., and Brudvig, G. W. (1998) in *Photosynthesis: Mechanisms and Effects* (G. Garab, Ed.) pp 1403−1406, Kluwer Academic Publishers, Dordrecht, The Netherlands.
9. Tang, X.-S., Randall, D. W., Force, D. A., Diner, B. A., and Britt, R. D. (1996) *J. Am. Chem. Soc. 118*, 7638−7639.
10. Szalai, V. A., and Brudvig, G. W. (1996) *Biochemistry 35*, 1946−1953.
11. Boussac, A., and Rutherford, A. W. (1988) *Biochemistry 27*, 3476−3483.
12. McLachlan, D. J., and Nugent, J. H. A. (1993) *Biochemistry 32*, 9772−9780.
13. Lakshmi, K. V., Eaton, S. S., Eaton, G. R., Frank, H. A., and Brudvig, G. W. (1998) *J. Phys. Chem. B 102*, 8327−8335.
14. Rhee, K.-H., Morris, E. P., Barber, J., and Kühlbrandt, W. (1998) *Nature 396*, 283−286.
15. Dorlet, P., Di Valentin, M., Babcock, G. T., and McCracken, J. L. (1998) *J. Phys. Chem. B 102*, 8239−8247.
16. Hasegawa, K., Kusunoki, M., Inoue, Y., and Ono, T.-a. (1998) *Biochemistry 37*, 9457−9465.
17. Rutherford, A. W. (1985) *Biochim. Biophys. Acta 807*, 189−201.
18. Rutherford, A. W., and Sétif, P. (1990) *Biochim. Biophys. Acta 1019*, 128−132.
19. Rutherford, A. W., and Acker, S. (1986) *Biophysics 49*, 101−102.
20. Babcock, G. T., Rodriguez, I. D., Hoganson, C., Sandusky, P. O., and El-Deeb, M. (1991) in *Spectroscopy of Biological Molecules* (Hester, R. E., and Girling, R. E., Ed.) pp 55−58, The Royal Society of Chemistry, Cambridge.
21. Brok, M., Horikx, J. T. G., and Hoff, A. J. (1986) *FEBS Lett. 203*, 36−40.
22. van Mieghem, F. J. E., Satoh, K., and Rutherford, A. W. (1991) *Biochim. Biophys. Acta 1058*, 379−385.
23. Kim, D. H., Britt, R. D., Klein, M. P., and Sauer, K. (1992) *Biochemistry 31*, 541−547.
24. Deligiannakis, Y., Tsekos, N., Petrouleas, V., and Diner, B. A. (1992) *Biochim. Biophys. Acta 1140*, 163−168.
25. Dismukes, G. C., and Sauer, K. (1978) *Biochim. Biophys. Acta 504*, 431−445.
26. Evelo, R. G., Nan, H. M., and Hoff, A. J. (1988) *FEBS Lett. 239*, 351−357.
27. Kamlowski, A., van der Est, A., Fromme, P., and Stehlik, D. (1997) *Biochim. Biophys. Acta 1319*, 185−198.
28. Kamlowski, A., Altenberg-Greulich, B., van der Est, A., Zech, S. G., Bittl, R., Fromme, P., Lubitz, W., and Stehlik, D. (1998) *J. Phys. Chem. B 102*, 8278−8287.
29. Kamlowski, A., Zech, S. G., Fromme, P., Bittl, R., Lubitz, W., Witt, H. T., and Stehlik, D. (1998) *J. Phys. Chem. B 102*, 8266−8277.
30. MacMillan, F., Hanley, J., van der Weerd, L., Knuepling, M., Un, S., and Rutherford, A. W. (1997) *Biochemistry 36*, 9297−9303.
31. Guigliarelli, B., Guillaussier, J., More, C., Sétif, P., Bottin, H., and Bertrand, P. (1993) *J. Biol. Chem. 268*, 900−908.
32. Un, S., Tang, X.-S., and Diner, B. A. (1996) *Biochemistry 35*, 679−684.
33. Schiller, H., and Iuzzulino, L. (1996) *Ber. Bunsen-Ges. Phys. Chem. 100*, 1999−2002.
34. Britt, R. D., Force, D. A., Campbell, K. A., Randall, D. W., Gilchrist, L. M. J., Clemens, K. L., Gingell, D. M., Peloquin, J. M., Pham, D. P., and Debus, D. J. (1998) in *Spectroscopic Methods in Bioinorganic Chemistry* (Solomon, E. I., and Hodgson, K. O., Ed.) pp 272−285, American Chemical Society, Washington DC.
35. Smith, P. J., Åhrling, K. A., and Pace, R. J. (1993) *J. Chem. Soc., Faraday Trans. 2 89*, 2863−2868.
36. Bittl, R., Zech, S. G., Fromme, P., Witt, H. T., and Lubitz, W. (1997) *Biochemistry 36*, 12001−12004.
37. Un, S., Brunel, L.-C., Brill, T. M., Zimmerman, J.-L., and Rutherford, A. W. (1994) *Proc. Natl. Acad. Sci. U.S.A. 91*, 5262−5266.
38. Berthold, D. A., Babcock, G. T., and Yocum, C. F. (1981) *FEBS Lett. 134*, 231−234.
39. Eaton, S. S., and Eaton, G. R. (1988) *Acc. Chem. Res. 21*, 107−113.
40. Eaton, S. S., More, K. M., Sawant, B. M., Boymel, P. M., and Eaton, G. R. (1983) *J. Magn. Reson. 52*, 435−449.
41. Boas, J. F., Hicks, P. R., Pilbrow, J. R., and Smith, T. D. (1978) *J. Chem. Soc., Faraday Trans. 2 74*, 417−431.
42. Schiller, H., Dittmer, J., Iuzzolino, L., Dorner, W., Meyer-Klaucke, W., Sole, V. A., Nolting, H. F., and Dau, H. (1998) *Biochemistry 37*, 7340−7350.
43. Blum, H., Salerno, J. C., and Leigh, J. S., Jr. (1978) *J. Magn. Reson. 38*, 385−391.
44. Eaton, G. R., and Eaton, S. S. (1989) *Biol. Magn. Reson. 8*, 339−397.
45. Zheng, M., and Dismukes, G. C. (1996) *Inorg. Chem. 35*, 3307−3319.
46. Svensson, B., Etchebest, C., Tuffery, P., van Kan, P., Smith, J., and Styring, S. (1996) *Biochemistry 35*, 14486-14502.
47. Koulougliotis, D., Tang, X.-S., Diner, B. A., and Brudvig, G. W. (1995) *Biochemistry 34*, 2850−2856.
48. Hirsh, D. J., and Brudvig, G. W. (1993) *J. Phys. Chem. 97*, 13216−13222.
49. Hoganson, C. W., and Babcock, G. T. (1992) *Biochemistry 31*, 11874−11880.
50. Mino, H., and Kawamori, A. (1994) *Biochim. Biophys. Acta 1185*, 213−220.
51. Chu, H. A., Nguyen, A. P., and Debus, R. J. (1994) *Biochemistry 33*, 6137−6149.
52. Diner, B. A., and Nixon, P. J. (1992) *Biochim. Biophys. Acta 1101*, 134−138.
53. Roffey, R. A., Kramer, D. M., Govindjee and Sayre, R. T. (1994) *Biochim. Biophys. Acta 1185*, 257−270.
54. Whitelegge, J. P., Koo, D., Diner, B., and Erickson, J. M. (1992) *Photosynth. Res. 34*, 140−140.
55. Chu, H. A., Nguyen, A. P., and Debus, R. J. (1995) *Biochemistry 34*, 5839−5858.

56. Mamedov, F., Sayre, R. T., and Styring, S. (1998) *Biochemistry 37*, 14245−14256.
57. Ghirardi, M. L., Lutton, T. W., and Seibert, M. (1998) *Biochemistry 37*, 13559−13566.
58. Hays, A. M. A., Vassiliev, I. R., Golbeck, J. H., and Debus, R. J. (1998) *Biochemistry 37*, 11352−11365.
59. Whitelegge, J. P., Koo, D., Diner, B. A., Domian, I., and Erickson, J. M. (1995) *J. Biol. Chem. 270*, 225−235.
60. Nixon, P. J., and Diner, B. A. (1994) *Biochem. Soc. Trans. 22*, 338−343.
61. Roffey, R. A., Vanwijk, K. J., Sayre, R. T., and Styring, S. (1994) *J. Biol. Chem. 269*, 5115−5121.
62. Yachandra, V. K., DeRose, V. J., Latimer, M. J., Mukerji, I., Sauer, K., and Klein, M. P. (1993) *Science 260*, 675−679.
63. Dole, F., Diner, B. A., Hoganson, C. W., Babcock, G. T., and Britt, R. D. (1997) *J. Am. Chem. Soc. 119*, 11540−11541.
64. Blondin, G., Davydov, R., Philouze, C., Charlot, M.-F., Styring, S., Åkermark, B., Girerd, J.-J., and Boussac, A. (1997) *J. Chem. Soc., Dalton Trans. 21*, 4069−4074.
65. Koulougliotis, D., Schweitzer, R. H., and Brudvig, G. W. (1997) *Biochemistry 36*, 9735−9746.
66. Nixon, P. J., and Diner, B. A. (1992) *Biochemistry 31*, 942−948.
67. Boerner, R. J., Nguyen, A. P., Barry, B. A., and Debus, R. J. (1992) *Biochemistry 31*, 6660−6672.
68. Manchanda, R., Brudvig, G. W., and Crabtree, R. H. (1995) *Coord. Chem. Rev. 144*, 1−38.
69. Wieghardt, K. (1994) *Angew. Chem., Int. Ed. Engl. 33*, 725−728.
70. Larson, E. J., and Pecoraro, V. L. (1992) in *Manganese Redox Enzymes* (Pecoraro, V. L., Ed.) pp 1−28, VCH, New York.
71. Limburg, J., Vrettos, J. S., Liable-Sands, L. M., Rheingold, A. L., Crabtree, R. H., and Brudvig, G. W. (1999) *Science 283*, 1524−1527.
72. Sussman, J. L., Lin, D., Jiang, J., Manning, N. O., Prilusky, J., Ritter, O., and Abola, E. E. (1998) *Acta Crystallogr., Sect. D 54*, 1078−1084.
73. Abola, E. E., Sussman, J. L., Prilusky, J., and Manning, N. O. (1997) Protein Data Bank Archives of Three-Dimensional Macromolecular Structures. in *Methods in Enzymology* (Carter, C. W. J., and Sweet, R. M., Ed.) pp 556−571, Academic Press, San Diego.
74. Tang, X.-S., Chisholm, D. A., Dismukes, G. C., Brudvig, G. W., and Diner, B. A. (1993) *Biochemistry 32*, 13742−13748.

BI990780S